Kurtz, C. D. Dzierba, W. G. Wirschun, J. D. Gleason, M. L. Snapper, A. H. Hoveyda, *J. Am. Chem. Soc.* **1999**, *121*, 4284; d) an enantioselective Strecker reaction catalyzed by cyclic peptide was previously reported: M. S. Iyer, K. M. Gigstad, N. D. Namdev, M. Lipton, *J. Am. Chem. Soc.* **1996**, *118*, 4910.

[7] A diastereoselective nitro-Mannich reaction was recently reported: H. Adams, J. C. Anderson, S. Peace, A. M. K. Pennell, *J. Org. Chem.* **1998**, *63*, 9932.

[8] Review: M. Shibasaki, H. Sasai, T. Arai, *Angew. Chem.* **1997**, *109*, 1290; *Angew. Chem. Int. Ed. Engl.* **1997**, *36*, 1236.

[9] The highest *ee* value we observed for *N*-isobutylidenebenzylamine was 14% *ee* (50% yield) using 20 mol% of [$LaLi_3$(binaphthoxide)$_3$] (LLB) as catalyst.

[10] a) H. Gröger, Y. Saida, H. Sasai, K. Yamaguchi, J. Martens, M. Shibasaki, *J. Am. Chem. Soc.* **1998**, *120*, 3089; b) Y. Hamashima, D. Sawada, M. Kanai, M. Shibasaki, *J. Am. Chem. Soc.* **1999**, *121*, 2641.

[11] W. B. Jennings, C. J. Lovely, *Tetrahedron* **1991**, *47*, 5561.

[12] *P,P*-Diphenylphosphinic amide (0.22 g, 1.0 mmol) was placed in a flame-dried 25-mL test tube and dissolved in CH_2Cl_2 (4.4 mL). To the solution was added benzaldehyde (0.20 mL, 2.0 mmol) and triethylamine (0.42 mL, 3.0 mmol), and then the mixture was cooled with an ice-water bath. A solution of $TiCl_4$ in CH_2Cl_2 (1.0 M, 0.55 mL) was added dropwise to the cooled mixture (over ca. 5 min). After the removal of the ice-water bath, the mixture was stirred for 2 h at room temperature, and then diluted with toluene (ca. 20 mL). The mixture was transferred into a 200-mL flask, and was diluted with further toluene (ca. 75 mL). The suspension was then filtered through celite, and the celite was washed with toluene. Evaporation of the solvent gave a brown oil containing mainly the imine **1a** and benzaldehyde. The excess benzaldehyde was removed under high vacuum, and recrystallization of the resulting solid provided the imine **1a** (0.26 g, 85%).

[13] For example, [$LaLi_3$(binaphthoxide)$_3$] (LLB) at $-40\,^{\circ}C$ gave the product in 29% yield and with 2% *ee*, and [AlLi(binaphthoxide)$_2$] (ALB) gave no product.

[14] When nitromethane was added in one portion, the result was less satisfactory (34% yield, 45% *ee*).

[15] This is a characteristic structure for heterobimetallic complexes with a Group 13 central metal.

[16] To overcome these problems of reactivity, bis(4-trifluoromethylphenyl)phosphinoyl imines were prepared. However, this strategy was unsuccessful, and did not give better results.

[17] Attempts to prepare the corresponding imines starting from enolizable aldehydes, such as isobutyraldehyde, failed due to self-condensation of the aldehydes under the conditions of imine formation.

[18] a) M. A. Sturgess, D. J. Yarberry, *Tetrahedron Lett.* **1993**, *34*, 4743; b) A. S. Kende, J. S. Mendoza, *Tetrahedron Lett.* **1991**, *32*, 1699.

[19] a) R. Ramage, B. Atrash, D. Hopton, M. J. Parrott, *J. Chem. Soc. Perkin Trans. 1* **1985**, 1217; b) R. Ramage, D. Hopton, M. J. Parrott, G. W. Kenner, G. A. Moore, *J. Chem. Soc. Perkin Trans. 1* **1984**, 1357.

[20] A. L. L. Duchateau, J. J. Guns, R. G. R. Kubben, A. F. P. van Tilburg, *J. Chromatogr. A* **1994**, *664*, 169.

[21] Address: 5-1-28, Chiyoda, Sakato, Saitama 350-02 (Japan); Fax: (+81) 492-84-1351.

[22] The enantiomeric excess of **2a** was determined by HPLC analysis on a chiral stationary phase (DAICEL Chiralcel OD, *i*PrOH/hexane 10/90, flow rate: 1.0 mL min^{-1}, retention time: 15 min (*S* isomer) and 27 min (*R* isomer), detection at 254 nm).

Mesoporous Magnetic Materials Based on Rare Earth Oxides**

Mitsunori Yada,* Hirohumi Kitamura, Akira Ichinose, Masato Machida, and Tsuyoshi Kijima

Since the discovery of the mesoporous silicas MCM-41[1] and FSM-16[2] derived from their surfactant mesocomposites, increasing attention has focused on the synthesis of mesoporous materials by the template method. Mesostructured silicas with surface-modified mesopores have large internal surface areas and narrow pore size distributions, and are effective catalysts and molecular sieves.[3] Mesoporous transition metal oxides are promising not only as catalysts and molecular sieves but also as highly functional materials with shape-specific and/or quantum effects characteristic of their ordered inorganic skeletons. Antonelli et al.[4] and Sun et al.[5] synthesized various micro- and mesoporous transition metal oxides such as niobium and tantalum oxides by the ligand-assisted liquid crystal template method with neutral primary amines. Layered[6] and hexagonal[7] mesostructured titanium oxides were found to be photocatalytically active.

Rare earth oxides and mixed oxides are useful as materials with luminescent, catalytic, electric, and magnetic properties that result from their 4f electrons. Rare earth garnets are applicable as bubble memory materials owing to their small magnetic domains with up or down spins. If such rare earth oxides were obtainable as mesoporous solids, they would be promising as adsorbents or separating agents with a combination of shape- or size-selectivity and magnetic properties. They could also act as electrically, magnetically, or optically functional host materials. We have reported the synthesis of a series of mesostructured metal oxides and demonstrated that the homogeneous precipitation method with urea is effective for the synthesis of aluminum-, gallium-, and yttrium-based dodecyl sulfate mesophases in which layered and hexagonal structures are templated by alkyl sulfate assemblies.[8–13] The hexagonal yttrium-based mesophase was converted into a mesoporous material with a specific surface area of 545 $m^2 g^{-1}$ by anion exchange of the surfactant with acetate ions, although the Al- and Ga-based analogues collapsed on the removal of surfactants.[13] However, the introduction of yttrium species into the inorganic framework of Al- and Ga-based mesophases yielded highly ordered mesoporous Al–Y and Ga–Y mixed oxides with specific surface areas of 798 and 714 $m^2 g^{-1}$, respectively.[14, 15] Here we report on the first synthesis and characterization of mesoporous rare earth oxides, as well as their anomalous magnetic properties.

The X-ray diffraction (XRD) pattern of the solid erbium-based mesophase isolated after a reaction time *t* of 3 h (see

[*] M. Yada, H. Kitamura, A. Ichinose, M. Machida, T. Kijima
Department of Applied Chemistry, Faculty of Engineering
Miyazaki University
Miyazaki, 889-2192 (Japan)
Fax: (+81) 985-58-2876
E-mail: t0g108u@cc.miyazaki-u.ac.jp

[**] This work was supported by a Grant-in-Aid for Encouragement of Young Scientists from the Ministry of Education, Scinence, Sports and Culture of Japan.

  1433-7851/99/3823-3506 $ 17.50+.50/0

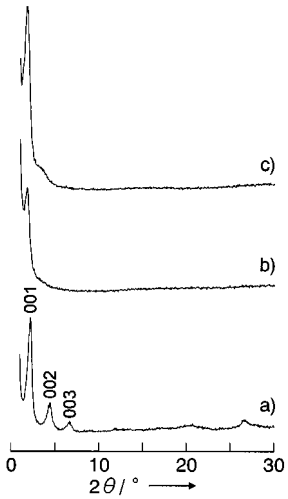

Figure 1. Powder X-ray diffraction (XRD) patterns of as-grown (a, b) and acetate-treated (c) samples of mesostructured erbium oxides isolated after reaction times of 3 (a) and 10 h (b,c).

Experimental Section) exhibited by three diffraction peaks at $2\theta = 2.2$, 4.4, and 6.7° (Figure 1a). The peaks are attributable to the (001), (002), and (003) reflections of a layered phase with an interlayer spacing of 4.0 nm. The observed interlayer spacing can be explained by assuming that the dodecyl sulfate molecules are arranged as a bilayer between the erbium-based inorganic layers. This is consistent with the transmission electron micrograph (Figure 2a), which shows stripes based on a layered structure, and the scanning electron micrograph, which indicates the formation of lamellar particles. The curved stripes and concentric patterns are characteristic of rare earth based layered mesophases. These specific patterns are similar to those observed for the yttrium oxide/surfactant[13] and aluminum phosphate/surfactant systems[16] but fundamentally different from the simple straight-extended layered structure of most layered mesostructured solids, such as the silica/surfactant[17] and zirconia/surfactant systems.[18]

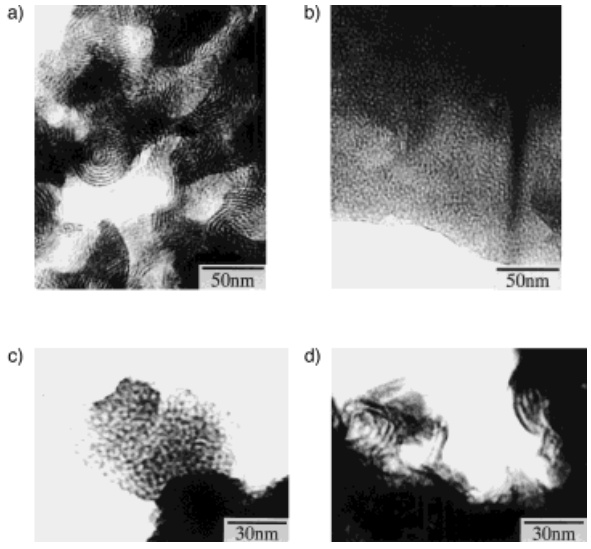

Figure 2. TEM images of the as-grown (a, b) and acetate-treated (c, d) mesostructured erbium oxides isolated after reaction times of 3 (a), 10 (b, d), and 20 h (c).

In contrast to the layered mesophase formed in the initial stage, the erbium-based mesophase obtained after a reaction time of 10 h showed a XRD pattern with one major peak at $2\theta = 1.8°$ and a weak broad band at $2\theta = 2-4°$ (Figure 1b). The d spacing given by the lowest angle diffraction peak increased from 4.0 nm for the initially formed layered mesophase to 4.9 nm for the mesophase formed after longer reaction times. The XRD pattern of the product after 10 h cannot be definitely assigned to the hexagonal or cubic structure. The transmission electron micrograph of this mesophase showed a hexagonal array of channels, but with less ordering (Figure 2b) than those of MCM-41 silica[1] and Al- and Ga-based mesophases,[8, 12] along with a stripe image, which suggests formation of a tubular rather than a cubic structure. The appearance of the less ordered structure could be explained by the transformation of the mesophase from the curled or concentric layered structure into a hexagonal structure that is highly modulated by the strained inorganic framework. The diffraction peak corresponding to $d = 4.9$ nm can most likely be assigned to the (100) reflection of a modulated hexagonal structure with a unit cell parameter of $a = 5.6$ nm. This is consistent with the broad band observed at $2\theta = 2-4°$, as expected for unresolved (110) and (200) reflections.

X-ray diffraction patterns indicative of a similar modulated hexagonal structure were observed for the Ho-, Tm-, Yb-, and Lu-based mesophases after a reaction time of 10 h. All of these XRD patterns are also similar to that of a hexagonal yttrium-based mesophase.[13] The Tb- and Dy-based mesophases obtained at $t = 10$ h also showed a XRD peak at nearly the same angle as above ($2\theta \approx 1.8°$), and the Gd-based mesophases were transformed from a layered structure ($t =$ 10 h) into a modulated hexagonal form at $t = 20$ h. These three mesophases indicated a relatively weak (100) peak, together with some peaks unassignable to the hexagonal structure. The XRD data also indicated the transformation of the Eu-based mesophase from a layered structure at $t = 10$ h into a mixture of layered and hexagonal forms at $t = 20$ h. These less crystalline hexagonal forms were unstable and were finally converted into the oxide dicarbonate hydrate in the case of Eu and into amorphous or unknown phases in the case of Gd, Tb, and Dy at $t = 30$ h. This is in marked contrast to the erbium and yttrium systems, in which the hexagonal structure is retained up to $t = 40$ h. The d of 4.7–5.3 nm spacing given by the lowest-angle diffraction peak for the hexagonal Gd–Lu mesophases were obtained from their XRD patterns (Table 1). The molar ratios of surfactant to rare earth element determined by X-ray microanalysis (XMA) were in the range 0.24–0.45 for the stable and metastable hexagonal mesophases. The IR spectra of the mesophases showed a broad band in the range of 1300–1700 cm^{-1} attributable to CO_3^{2-}, along with some peaks assignable to dodecyl sulfate; hence, the mesophases are composed of rare earth oxide hydroxide, carbonate, and dodecyl sulfate species. The La, Ce, Pr, Nd, and Sm systems all yielded layered mesophases with an interlayer spacing of 3.6 nm as the major phase at $t = 10$ h. These layered mesophases were converted into $Ce_2O(CO_3)_2 \cdot H_2O$, $PrCO_3OH$, $NdCO_3OH$, and $Sm_2O(CO_3)_2 \cdot xH_2O$, respectively, along with residual layered phase after 30 h. In the case of La, the product was still composed mainly of the layered mesophase and only partially of $La_2O(CO_3)_2 \cdot xH_2O$ even after 30 h. These layered phases are more highly crystalline than the Er- and Y-based layered mesophases. As a typical case, the XRD patterns of the neodymium-based solids isolated from reactions at $t = 10$ h and $t = 30$ h are shown in Figure 3.

  1433-7851/99/3823-3507 $ 17.50+.50/0

Table 1. Characterizations of the as-grown and acetate-treated mesostructured rare earth oxides.

Rare earth element	Atomic number	As-grown		Anion-exchanged				
		d_{max} [nm][a]	S/M [mol mol^{-1}]	d_{max} [nm][a]	specific surface area [m^2 g^{-1}]	magnetic susceptibility [10^{-4} emu g^{-1}]	relative magnetic suceptibility	relative μ_{eff}^2[c]
Gd	64	4.9	0.24	4.9	287	0.55	0.33	0.54
Tb	65	5.0	0.39	5.1	348	1.56	0.93	0.83
Dy	66	5.3	0.43	5.1	253	1.66	1.00	1.00
Ho	67	4.9	0.45	5.1	316	1.62	0.97	1.00
Er	68	4.9	0.44	4.9	280	1.23	0.73	0.85
Tm	69	4.9	0.37	4.9	335	0.86	0.52	0.50
Yb	70	4.9	0.32	4.9	283	0.66	0.40	0.18
Lu	71	4.7	0.32	4.7	257	0	0	0

[a] The d spacing was determined from the lowest angle diffraction peak. [b] S/M = [surfactant]/[rare earth element]. [c] μ_{eff} is the theoretical magnetic moment of the free trivalent cation.

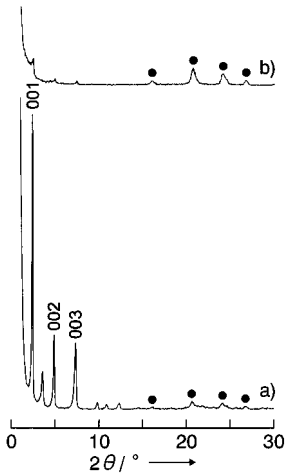

Figure 3. XRD patterns of neodymium oxides isolated after reaction times of 10 (a) and 30 h (b). ●: $NdCO_3OH$.

This layer to hexagonal transition can be explained in terms of interlayer condensation and subsequent molecular rearrangement of the surfactant. The increase in pH due to decomposition of urea would result in interlayer condensation and cross-linking between adjacent rare earth oxide hydroxide clustered layers. This would proceed cooperatively with partial release of the surfactant molecules and their rearrangement into a more stable rodlike assembly. The rare earth cations of small ionic radius (Y, Ho to Lu) yield a modulated hexagonal mesophase as the most stable phase by structural transformation of a layered mesophase, whereas the medium-sized (Eu to Dy) and large (La to Sm) cations initially form a layered mesophase that finally undergoes conversion into a carbonate or other phase with and without an intermediate layer to hexagonal transition, respectively. This classification of the rare earth elements is analogous to the classification of their sesquioxides into the La_2O_3 (Type A), Sm_2O_3 (Type B), and Sc_2O_3 (Type C) crystal structures.[19, 20]

The hexagonal mesophases were subjected to anion exchange with acetate ions[21] to remove the incorporated surfactants. The XRD patterns of the acetate-treated mesophase all showed a single peak at $2\theta \approx 1.8^\circ$ assignable to the (100) reflection and a shoulder at $2\theta = 2-4^\circ$ associated with the (110) and (200) reflections of a hexagonal structure, as exemplified for Er in Figure 1c and for Gd–Lu in Figure 4. These patterns are similar to those of the as-grown phases, but with a more distinct shoulder. The d spacings determined for the lowest-angle diffraction peak were barely changed by treatment with acetate (Table 1). The transmission electron micrograph of the Er product showed a hexagonal array of channels, but with less ordering (Figure 2c), and a stripe image (Figure 2d) suggestive of the existence of tubular pores, similar to the as-grown mesophase. No sulfur-containing species were detected by XMA on the acetate-treated solids. These XRD, TEM, and XMA results indicate that the dodecyl sulfate anions are completely exchanged with acetate anions and that the modulated hexagonal structure is retained. Anion exchange may be driven by the larger hydrophobic attraction between the long-chain dodecyl sulfate ions and ethanol molecules.

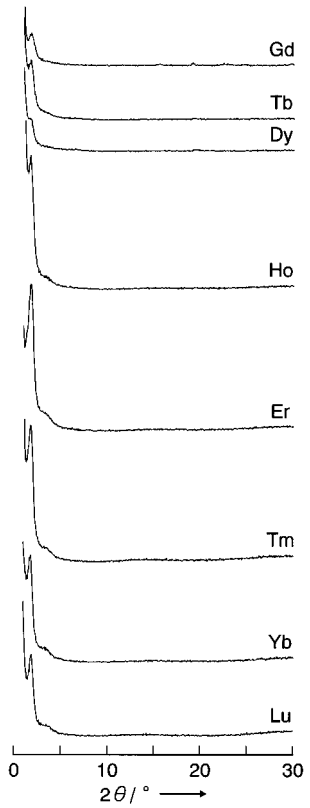

Figure 4. XRD patterns of acetate-treated rare earth oxides isolated after reaction times of 10 (Tb, Dy, Ho, Er, Tm, Yb, Lu) and 20 h (Gd, Tb).

The N_2 adsorption isotherm of the anion-exchanged erbium mesophase showed two distinct regions (Figure 5). The N_2 adsorption in the range $P/P_0 = 0-0.2$ is due to monolayer coverage of the mesopores and the surface of the particles, whereas that in the range $P/P_0 = 0.2-0.4$ is characteristic of capillary condensation in mesopores. The desorption isotherm showed no hysteresis relative to the adsorption isotherm, and this indicates that little irreversible interaction occurs between N_2 and the mesopores. Given the $ErO_{1.5}$ to SiO_2 mass ratio of 191.3/60.1, the mesoporous erbium oxide with a specific surface area of 280 m^2 g^{-1} corresponds to a mesoporous silica with a specific surface area of 891 m^2 g^{-1}. This is nearly equal to that 1000 m^2 g^{-1} for MCM-41 or FSM-16. A similar N_2 adsorption isotherm was observed for all other anion-exchanged mesophases. Their specific surface areas are in the range of 253–348 m^2 g^{-1} (Table 1). The effective pore sizes of 2.5–3.0 nm for the anion-exchanged solids were obtained from the pore size distributions (Figure 5). On the basis of the above XRD, TEM, and N_2 adsorption data, we conclude that the anion-

  1433-7851/99/3823-3508 $ 17.50+.50/0

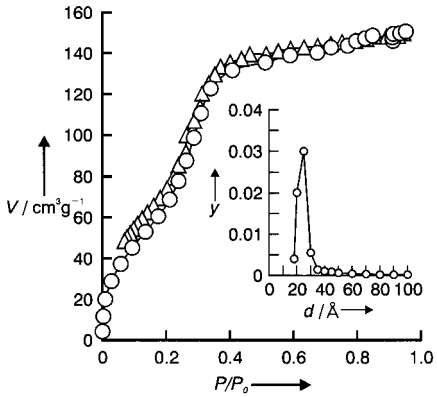

Figure 5. N_2 adsorption (○) and desorption (△) isotherms and pore size distribution (inset) of the acetate-treated mesostructured erbium oxide isolated after a reaction time of 10 h. $y = \Delta V/\Delta d$ [mL g^{-1} Å^{-1}(STP)].

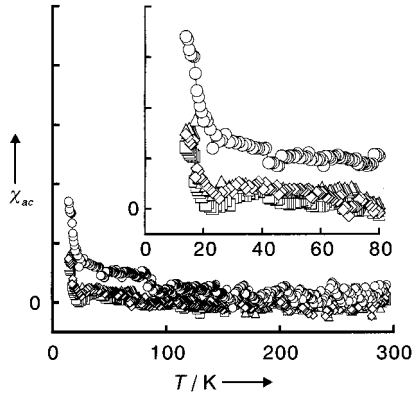

Figure 6. Plots of the ac magnetic susceptibility χ_{ac} against temperature for the bulk (○), layered (□), as grown hexagonal (△) and acetate-treated hexagonal (◇) mesostructured erbium oxides.

exchanged products are porous materials with highly ordered mesopores.

At room temperature, the magnetic susceptibilities of the layered and modulated hexagonal erbium-based surfactant mesophases and of the acetate-exchanged mesoporous erbium oxide were 0.68×10^{-4}, 1.03×10^{-4}, and 1.23×10^{-4} emu g^{-1}, respectively, corresponding to 35, 53, and 64% of the value of 1.94×10^{-4} emu g^{-1} for reagent-grade erbium oxide. The magnetic susceptibility ratio of 0.64 for the erbium mesophase relative to bulk erbium oxide is in good agreement with its weight fraction of Er_2O_3 of 0.65, as determined by thermogravimetric analysis (TGA). The magnetic susceptibility ratios of 0.35 and 0.53 for the layered and hexagonal mesophases relative to bulk erbium oxide are less than the weight fractions of Er_2O_3 of 0.45 and 0.57, respectively. Here the dodecyl sulfate to Er molar ratios of the layered and hexagonal mesophases are 2.11 and 0.44, respectively. It is therefore most likely that the magnetic susceptibility of the mesostructured solids, layered or modulated hexagonal, is little affected by the bonding of acetate ions to the rare earth cations, but significantly decreased by the influence of the sulfate groups of incorporated surfactant. The magnetic susceptibility of the rare earth oxide based mesoporous materials is on the order of 10^{-4} emu g^{-1} and ranges from 0.55×10^{-4} emu g^{-1} for Gd to 0 emu g^{-1} for Lu via a maximum value of 1.66×10^{-4} emu g^{-1} for Dy (Table 1). The relative magnetic susceptibilities for the mesoporous solids are also in agreement with the relative values of the squares of theoretical magnetic moments of the corresponding rare earth ions in their free trivalent states[20] (Table 1). These facts suggest that the mesoporous oxides are paramagnetic materials with rare earth ions in nearly the same electron spin state as in their free trivalent ions. However, in contrast to the typical paramagnetic behavior of bulk erbium oxide, the ac magnetic susceptibility versus temperature curves of the mesostructured rare earth oxides showed a significant minimum near 23–25 K, regardless of whether their structural types is layered or hexagonal, and as-grown or acetate-exchanged (Figure 6). This magnetic anomaly resembles that of spin glasses or mictomagnetic materials and indicates that the paramagnetic ordering of spins at low temperature is decrystallized by a specific effect due to the mesostructural arrangement of rare earth ions.

Experimental Section

The mesostructured rare earth oxides were synthesized by the homogenous precipitation method with urea. Urea was used to raise the pH value of the solution, because on heating at above 60 °C it undergoes hydrolysis [Eq. (1)].

$$(NH_2)_2CO + 3H_2O \rightarrow 2NH_4^+ + 2OH^- + CO_2 \quad (1)$$

Nitrates of La, Ce, Pr, Nd, Sm, Gd, Dy, Er, Yb, and Lu and chlorides of Eu, Tb, Ho, and Tm were used as rare earth element sources. The structural and morphological properties of the products were little affected by whether nitrate or chloride was the counterion.[11] Sodium dodecyl sulfate (SDS) $CH_3(CH_2)_{11}OSO_3Na$ was used as templating agent. Rare earth metal nitrate or chloride, SDS, urea, and water were mixed in a molar ratio of 1:2:30:60 and stirred at 40 °C for 1 h to yield a transparent mixed solution. The mixed solution was heated to 80 °C and then kept at that temperature. The pH value of the reaction mixture increased due to the hydrolysis of urea, and precipitation occurred. After a reaction time of 3, 10, 20, and 30 h, the resulting mixture was immediately cooled to room temperature to prevent further hydrolysis of urea. After centrifugation, the solid was washed with water a few times and then dried in air.

The surfactant was removed from the mesophases by anion exchange with acetate ions.[21] The solid (0.5 g) was mixed with a 0.05 M ethanolic solution of sodium acetate (40 mL) and stirred at 40 °C for 1 h. The resulting solids were washed with ethanol and dried in air.

Powder X-ray diffraction (XRD) measurements were performed on a Simadzu XD-D1 diffractometer with $Cu_{K\alpha}$ radiation. The IR absorption spectra were measured on KBr pellets with a Nippon Bunko FT/IR-300. Transmission electron microscopy (TEM) was carried out on a Hitachi H-800MU instrument. Scanning electron microscopy (SEM) was performed on a Hitachi H-4100. X-ray micro analysis (XMA) was conducted on a HORIBA EMAX-5770 instrument. Specific surface area was measured by the BET method with N_2.[22] Pore size distributions was determined by the Cranston Inkley method.[23] Thermogravimetric and differential thermal analysis (TG-DTA) was conducted with a SEIKO TG/DTA320U at 10 °C min^{-1}. The dc and ac magnetic susceptibilities were measured by the field vibration method on a Rikendennshi BHV-35HT magnetometer and by the self-inductance method with a Kokuyo KC-533 LCR meter, respectively.

Received: June 10, 1999 [Z13541IE]
German version: *Angew. Chem.* **1999**, *111*, 3716–3720

Keywords: magnetic properties · mesophases · mesoporosity · rare-earth compounds · template synthesis

  1433-7851/99/3823-3509 $ 17.50+.50/0

[1] C. T. Kresge, M. E. Leonowicz, W. J. Roth, J. C. Vartuli, J. S. Beck, *Nature* **1992**, *359*, 710.
[2] T. Yanagisawa, T. Shimizu, K. Kuroda, C. Kato, *Bull. Chem. Soc. Jpn.* **1990**, *63*, 988.
[3] K. Moller, T. Bein, *Chem. Mater.* **1998**, *10*, 2950.
[4] D. M. Antonelli, J. Y. Ying, *Angew. Chem.* **1996**, *108*, 461; *Angew. Chem. Int. Ed. Engl.* **1996**, *35*, 426.
[5] T. Sun, J. Y. Ying, *Nature* **1997** *389*, 704.
[6] H. Fujii, M. Ohtaki, K. Eguchi, *J. Am. Chem. Soc.* **1998**, *120*, 6832.
[7] V. F. Stone, Jr., R. J. Davis, *Chem. Mater.* **1998**, *10*, 1468.
[8] M. Yada, M. Machida, T. Kijima, *Chem. Commun.* **1996**, 769.
[9] M. Yada, H. Hiyoshi, K. Ohe, M. Machida, T. Kijima, *Inorg. Chem.* **1997**, *36*, 5565.
[10] M. Yada, H. Kitamura, M. Machida, T. Kijima, *Langmuir* **1997**, *13*, 5252.
[11] M. Yada, H. Kitamura, M. Machida, T. Kijima, *J. Porous Mater.* **1998**, *5*, 133.
[12] M. Yada, H. Takenaka, M. Machida, T. Kijima, *J. Chem. Soc. Dalton Trans.* **1998**, 1547.
[13] M. Yada, H. Kitamura, M. Machida, T. Kijima, *Inorg. Chem.* **1998**, *37*, 6470.
[14] M. Yada, M. Ohya, M. Machida, T. Kijima, *Chem. Commun.* **1998**, 1941.
[15] M. Yada, M. Ohya, M. Machida, T. Kijima, unpublished results.
[16] A. Chenite, Y. L. Page, V. R. Karra, A. Sayari, *Chem. Commun.* **1996**, 413.
[17] G. S. Attard, J. C. Glyde, C. G. Göltner, *Nature* **1995**, *378*, 366.
[18] Y. Huang, W. M. H. Sachtler, *Chem. Commun.* **1997**, 1181.
[19] V. M. Goldschmidt, F. Ulrich, T. Barth, *Skr. Nor. Vidensk. Akad. Kl. 1* **1925**, *5*, 1.
[20] I. Warshaw, R. Roy, *J. Phys. Chem.* **1961**, *65*, 2048.
[21] B. T. Holland, P. K. Isbester, C. F. Blanford, E. J. Munson, A. Stein, *J. Am. Chem. Soc.* **1997**, *119*, 6796.
[22] S. Brunauer, P. H. Emmett, E. Teller, *J. Am. Chem. Soc.* **1938**, *60*, 309.
[23] R. W. Cranston, F. A. Inkley, *Adv. Catal.* **1957**, *9*, 143.

On the "Rebound" Mechanism of Alkane Hydroxylation by Cytochrome P450: Electronic Structure of the Intermediate and the Electron Transfer Character in the Rebound Step**

Michael Filatov, Nathan Harris, and Sason Shaik*

Alkane hydroxylation is a key process by which the heme enzyme cytochrome P450 metabolizes xenobiotics.[1] The consensus mechanism (Scheme 1), called the rebound mechanism,[2] proceeds by an initial hydrogen abstraction from the alkane (RH) by the active ferryl–oxene species ($Por^{+\bullet}Fe^{IV}{=}O$), to form a radical R$^\bullet$ and a hydroxo–iron complex as intermediates (step a). Subsequently the radical rebounds on the hydroxy group and generates the ferric–alcohol complex (step b). This mechanism is currently under debate due to recent mechanistic studies,[3] using ultrafast radical clocks to probe the presence of a free radical, that suggest a concerted oxene-insertion mechanism. Nevertheless, quite a few investigations do report results which are consistent with the rebound mechanism.[2, 4] As such, the mechanism of a very important reaction in the vital system remains not fully resolved.

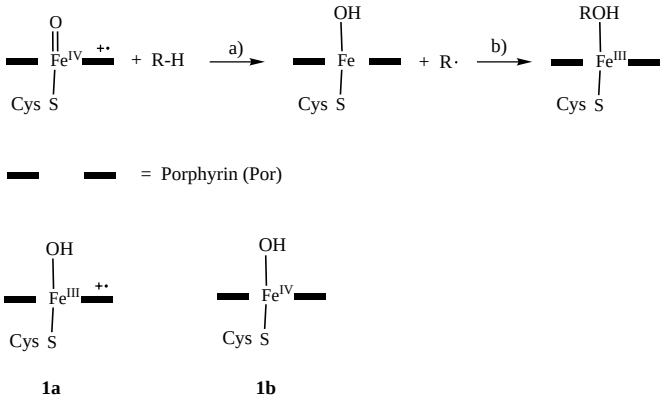

Scheme 1. Schematic representation of the rebound mechanism, and of the two electromeric forms (**1a** and **1b**) of the hydroxo–iron intermediate.

A great deal of mechanistic research has traditionally focused on whether the radical intermediate exists or not, while very few studies have addressed the nature of the hydroxo–iron species **1** (Scheme 1).[5] It is important to address the electronic structure of this intermediate, since this has bearing on its reactivity in the rebound step, and hence on an eventual resolution of the mechanistic dilemma as a whole. The ferryl–hydroxo species may exist in two electromeric[6] forms. In one (**1a**, Scheme 1) the iron appears as a Fe^{III} center to provide a cation radical porphyrin, while the other (**1b**) contains high-valent Fe^{IV} with a neutral porphyrin.[5, 7] The spin state of the complex may be low ($S=1$), intermediate ($S=2$), or high ($S=3$).[7c] In addition, due to available alternative occupation modes of the d-orbital block, and of the porphyrin's orbitals (the a_{1u} and a_{2u} types[8]), there might exist a few closely lying states with different state symmetries. The present paper uses density functional and model solvent calculations to resolve this complex state situation for the hydroxo–iron species, and addresses due implications on the rebound mechanism.

All calculation were performed by use of the JAGUAR 3.5 package.[9] Benchmark calculations showed that the pure density functional BP86[10a] and the hybrid (HF/DFT) functional B3LYP levels[10b] give the same stability ordering for the two electromers, and therefore the rest of the study was performed with B3LYP. Based on previous experience with the oxo iron porphyrin,[8] reliable spin state ordering of organometallic species can be obtained with moderate basis sets, but geometry optimization is essential since different spin situations may have very different bond lengths between iron and the axial ligands. On iron we used the Los Alamos effective core potential coupled with the double zeta LACVP basis set,[11] while for the rest of the atoms we utilized the 6-31G basis set. The latter basis set was ascertained against a calculation that used the more flexible LACV3P basis set[11]

[*] Prof. S. Shaik, Dr. M. Filatov, Dr. N. Harris
Department of Organic Chemistry and
The Lise Meitner-Minerva Center for
Computational Quantum Chemistry
Hebrew University, 91904 Jerusalem (Israel)
Fax: (+972) 2-6585345
E-mail: sason@yfaat.ch.huji.ac.il

[**] This research was sponsored by the Volkswagen Stiftung and The Israeli Science Foundation (ISF). S.S. thanks the Humboldt Foundation for a Senior Research Award.

  1433-7851/99/3823-3510 $ 17.50+.50/0